applied sciences

MDPI

Article

k_f Evaluation in GFRP Composites by Thermography

Marta De Giorgi [1,*], Riccardo Nobile [1] and Fania Palano [2]

[1] Department of Engineering for Innovation, University of Salento, 73100 Lecce, Italy; riccardo.nobile@unisalento.it
[2] ENEA, Centro Ricerche di Brindisi, c/o Cittadella della Ricerca S.S.7 Appia km 706, 72100 Brindisi, Italy; fania.palano@enea.it
* Correspondence: marta.degiorgi@unisalento.it

Abstract: Since the presence of a notch in a mechanical component causes a reduction in the fatigue strength, it is important to know the k_f value for a given notch geometry and material. This parameter is fundamental in the fatigue design of aeronautical components that are mainly made of composites. k_f is available in the literature for numerous types of notch but only for traditional materials such as metals. This paper presents a new practice, based on thermographic data, for the determination of the fatigue notch coefficient k_f in composite notched specimens. The innovative aspect of this study is therefore to propose the application on composite materials of a new thermographic procedure to determine k_f for several notch geometries: circular, U and V soft and severe notches. It was calculated, for each type of notch, as the ratio between the fatigue limits obtained on the cold and hot zone corresponding to the smooth and notched specimen, respectively. Consequently, this research activity provides, for the first time, a little database of k_f for two particular typologies of composite materials showing a fast way to collect further values for different laminates and notch geometries.

Keywords: composites; fatigue; geometric effect; notch sensitivity; thermography

Citation: De Giorgi, M.; Nobile, R.; Palano, F. k_f Evaluation in GFRP Composites by Thermography. *Appl. Sci.* **2021**, *11*, 5200. https://doi.org/10.3390/app11115200

Academic Editor: Carosena Meola

Received: 6 May 2021
Accepted: 28 May 2021
Published: 3 June 2021

1. Introduction

A critical aspect of standard test methods for fatigue characterization is the lack of any information on heat dissipation in the material and the very expensive experimental campaigns in terms of time and costs. Thermal methods represent valid support to study fatigue behaviour of materials, since they allow both the reduction of time and costs of the experimental campaigns and the possibility to estimate damage phenomena correlated to dissipative heat sources developed during fatigue. The fatigue crack develops with consequent generation of thermal energy, which can be considered as the effect of a plausible activation mechanism of the crack, which is therefore correlated with the fatigue limit. Based on this correlation, Risitano proposed an alternative method for the evaluation of the fatigue limit through the use of infrared thermography [1–3]. Risitano's method has the peculiarity consisting of a rapid estimation of this important material property.

The use of this technique, in addition to the advantages of thermography, such as the possibility of providing real-time information on the monitored area temperature, the minimum preparation of the specimen and the possibility of not breaking it, involves, in theory, the use of a single specimen for the evaluation of the fatigue limit, which results in a saving in terms of time and cost of the test. The thermographic technique allows obtaining slightly lower fatigue limit values compared with the Stair-Case method and represents a potential non-destructive characterization technique for prediction of fatigue behaviour even of complex shape and in-service components.

A lot of works in scientific literature apply thermal methods for a fast determination of the fatigue limit in metal materials, especially in steels [1–10]. Among these, only a few papers consider the influence of a notch presence, which is a region with high-stress concentration, in these materials [8,9]. An automatic thermal data analysis procedure

has been proposed for fatigue limit evaluation of martensitic and precipitation hardening stainless steel [4,5]. The thermal rapid determination of fatigue limit for stainless steel has been achieved, by comparing temperature and energy-based approaches available in the literature [6]. A Quantitative Thermographic Method has also been proposed for residual fatigue life assessment of mild steel for specimens with a central flat-bottom hole [7]. Thermographic method based on an iterative procedure has been applied to Fe 510 standard and notched specimens with semi-circular notch, obtaining the fatigue limit as the intersection of the two straight lines interpolating experimental thermographic data corresponding to stresses below and above the fatigue limit [8]. A large amount of fatigue data, referred to AISI 304L smooth and V-notched specimens, were represented in a single scatter band considering the specific heat loss per cycle as a damage parameter [9]. Thermographic approach to estimate the fatigue limit of 3 stainless steel specimens, exhibiting fully austenitic, fully martensitic and duplex biphasic microstructure, has been proposed [10].

Despite the metallic materials case, a lot of scientific researches consider the fatigue damage monitoring by thermal methods in composite materials [11–17], but only some of these attempt to evaluate the fatigue limit [13,16]. The application of IR-thermography to different glass and basalt fibre-reinforced composite materials, to relate their thermal response to the mechanical behaviour, is presented in [11]. An analytical model based on cumulative damage was adopted for predicting the damage evolution in carbon/epoxy composite material obtaining a relation between the heat dissipation and damage [12]. An energy-based approach is proposed to analyse the fatigue strength of plain and notched specimens in short fibre-reinforced plastic. The energy per cycle dissipated as heat by a unit volume of material is assumed as a fatigue damage indicator, obtaining that this parameter can be correlated to the fatigue strength independently of the geometry, despite some limitations for severe notches [13]. Research focusing on GFRP aimed to study its fatigue behaviour from both the mechanical and the thermal points of view [14]. In order to perform the fatigue characterization of GFRP composite materials, two methods have been presented for determining fatigue limit: a statistical method validated for metallic materials and a graphical method applied on phase data, both showing a good agreement with the conventional S-N curve [15]. A technique to pass from temperature information to distribution of heat sources on the composites surface to monitor the damage evolution of some carbon/epoxy composite specimens during a fatigue test has been proposed [16]. Only one study analysed the influence of a particular type of notch as a central hole [17] but no study has analysed the presence of notch with different geometries in composites. The aim of this previous study was to understand the damage evolution of unidirectional GFRP specimens with and without a circular notch under static and fatigue loads, by observing the thermal phenomena on the external surface of the GFRP composite [17].

At present, the research world is showing a growing interest in studying the mechanical behaviour of composites, employing both traditional and innovative techniques, with the final purpose of making previsions regarding their service life. A commonly used approach is based on the assessment of the temperature plateau during a stepwise loading procedure. The composite structures' fatigue failure is generally caused by a combination of different types of damage: fibre breakage, matrix cracking, delamination, ply failure or debonding. Each of these mechanisms is amplified by stress concentrations due to manufacturing defects, cut-outs, notches and flaws. Most of the structural components in the automotive and aerospace applications present notches or holes causing a stress concentration that reduces the overall fatigue strength in the material that is generally a composite material. In machines and structures, in fact, progressive local failure often takes place at the root or in the proximity of the notches or holes.

This paper presents a new application of the Risitano method [1,9] for the determination of the fatigue notch coefficient k_f in GFRP composite specimens. Traditionally, the fatigue notch effect k_f is obtained by the ratio between two fatigue limits, referred to un-notched and notched specimen. As a consequence, two fatigue curves are needed to define this parameter for each geometry. It is evident that the approach commonly used

for homogeneous materials to define k_f is inapplicable in the case of composite, not only for the entity of the experimental effort, but also for the lack of generality of the approach. Assuming to have determined the notch effect k_f for a specific geometry carrying out experimental fatigue tests on a selected layup sequence, in fact, it would be not possible to extend the result to specimen having the same notch geometry but a different ply sequence. Therefore, the development of a methodology for the rapid determination of k_f would be useful. Using a thermographic approach, the fatigue limit could be evaluated using a stepped fatigue test. Adopting this technique both for the un-notched and notched section, it is possible to determine these two fatigue limits and the corresponding notch fatigue coefficient k_f using a unique specimen. This last parameter will be defined simply by the ratio between the fatigue limits corresponding to the net and gross section determined using the Risitano method [1–3]. Since fatigue tests are carried out only on a single notched specimen, the advantage of the methodology is evident. In this work, this technique has been proposed to study different composite specimens with different notch geometries and layup, which have been tested under tension–tension fatigue load. Particularly, GFRP composite specimens characterized by circular, U, smooth and sharp V notch geometries were tested in order to determine the corresponding notch fatigue coefficient k_f.

In detail, Risitano's method consists of a "load step test" that indicates a fatigue test in which the stress has constant amplitude for each step, and it increases in the subsequent steps. Then, the stress amplitude of the step, σ_a, and the corresponding value of the temperature increase, respect to the initial value, ΔT, are reported on a diagram ΔT-σ_a. Monitoring a stepped test through a thermal camera, it is possible to diagram the temperature trend for the duration of the test. If the number of cycles is high enough, a particular trend is obtained (see Figure A1 in Appendix A).

If the value of the applied stress is below the fatigue limit, the temperature of the area under examination increases during the first part of the test (stage I), then remains constant (stage II) until before breaking, followed by a rapid increase in temperature (stage III). The duration of the stages, in terms of the number of cycles, is influenced by the level of the applied load. Experience shows that for loads lower than the yield point, the duration of the first stage is approximately 10% of the break life, while for loads close to yielding, the second stage is practically absent or very limited. Concerning the temperature rise speed, identifiable with the slope of the first part of the curve, it is higher as the applied load value increases.

For each stress amplitude, and therefore for each step, it is possible to determine the limit temperature. By plotting the value of this temperature for each step on a diagram, a series of points is obtained (see Figure A2 in Appendix A). Risitano rapid method consists of tracing two asymptotes on the above-mentioned diagram [1–3]. The intersection of these lines will identify the value of the fatigue limit on the abscissa axis. This method stems from the fact that the fatigue limit can be defined, in a macroscopic way, as the value of the stress when the temperature increases on the specimen surface is zero [1].

Based on previous considerations, if these characteristic parameters are plotted against the applied load, the fatigue limit falls on the abscissa axis, having imposed $\Delta T = 0$ (or $\Delta T/\Delta N = 0$). The first asymptote is thus determined.

Subsequently, it is necessary to investigate the steps that show an increase in temperature that deviates significantly from the previous value, where significant means higher than a minimum value corresponding to the experimental noise, quantifiable by statistical means. At this point, it needs to draw the straight line that best approximates the trend of the data and is, therefore, representative of the trend change. To do this, a dispersion band is determined within which the greatest number of points are expected to fall. The intersection of the regression line, representing the second asymptote, with the abscissa axis, identifies the fatigue limit value. The determination of the dispersion band arises from statistical observations, in which it is assumed that the data are distributed according to a Gaussian curve with an 80% confidence rate.

The experience gained on the technique shows that during the interpolation process it is appropriate to exclude the points where the increase in temperature is very high. This is because as the load increases, i.e., approaches the fatigue limit, phase II is very short or even absent, so the three phases of the curve are not clearly distinguishable. In this case, therefore, one cannot speak of "stabilization temperature".

The measurement of the stabilization temperature requires the achievement of a high number of cycles, such that the accumulation of damage on the next step cannot be overlooked. The truncation to the number of cycles belonging to stage I, however, does not allow knowing the limit temperature. In the following, authors adopted an analytical model that allows estimating the value of this temperature from the experimentally collected data.

2. Materials and Methods

The determination of the stabilization temperature is based on several considerations. The surface of the specimen, which is the border between the specimen and the environment, is subject to a double heat exchange; in fact, on one hand, it absorbs the heat generated in the innermost parts of the specimen where the damage occurs; on the other hand, it transfers heat to the external environment, which is at a lower temperature. The surface temperature trend is therefore given by the balance between these two phenomena. The equation that governs heat transfer phenomena is the heat transfer law, or Newton's law, and it has the following Expression (1):

$$\frac{Q}{\Delta t} = -h \cdot S \cdot (T(t) - T_a) \tag{1}$$

where:

- Q is the amount of heat generated inside the specimen at the instant of time Δt;
- h is the transport or external conductivity coefficient, which depends on the nature of the body and the environment, the state of the contact surfaces and the environmental conditions;
- S is the thermal exchange surface;
- T_a is the temperature of the reference body, very often the environment;
- $T(t)$ is the temperature of the body that is releasing heat at the instant t.

The minus sign indicates that there is heat transfer to the environment if $T(t) > T_a$ and vice versa if $T(t) < T_a$.

The solution of this differential equation is the typical one of the first order, namely:

$$T(t) = T_0 + \left(1 - e^{-\frac{1}{\tau}}\right) \cdot (T_1 - T_0) \tag{2}$$

where T_0 is the initial temperature. In terms of temperature variation, it is possible to rewrite the equation in the following way:

$$\Delta T(t) = \left(1 - e^{-\frac{t}{\tau}}\right) \cdot \Delta T_1 \tag{3}$$

where:

τ is a constant indicating the speed of heat exchange;

$\Delta T(t)$ is the increase in surface temperature at the instant t;

ΔT_1 is the difference between T_1, which is the limit temperature, and T_0. The stabilization value, indeed, is given by:

$$\lim_{t \to \infty} \Delta T(t) = \Delta T_1 \tag{4}$$

The value of ΔT_1 is determined employing a best-fit operation. Interpolating the temperature values captured by the thermal camera with the function $\Delta T(t)$ of Eqution (3),

the regression coefficients ΔT_1 and τ will be calculated. This procedure thus avoids the impossibility of measuring the limit temperature experimentally.

A routine in Matlab was used to process the thermal imaging camera acquisitions and to generate the thermal maps and the graphs for a first check of data. A further routine in Mathematica was used to exclude possible errors in the experimental data, such as drift or shift of the data, and to calculate the regression coefficients.

The analysed material is an E-glass/epoxy composite. The specimens are obtained from two laminates, realized by the vacuum bag moulding technique, with a ply sequence of four fabric layers. The first one has a resulting thickness b of 2.2 mm and a ply sequence of four biaxial fabric layers with stacking sequence $[0\ 90\ 90\ 0]_{x4}$, while the second one has a thickness b of 4 mm and a ply sequence of four quadriaxial fabric layers with stacking sequence $[0\ +45\ 90\ -45]_{x4}$.

The physical and mechanical properties of the constituent materials are shown in Table 1. Specimens were obtained from panels 1 and 2 according to the standard ASTM D3039 [18] and they were provided with opportune tabs allowing an efficient load transmission during test and avoiding, at the same time, damage of specimen caused by the grip system of the test machine.

Table 1. Physical and mechanical properties of the laminate constituent materials.

Laminate 1 [0 90 90 0]		***Laminate 2 [0 +45 90 −45]***	
E-Glass		**E-Glass**	
Diameter	10 μm	Diameter	14 μm
Young modulus	73,000 MPa	Young modulus	72,500 MPa
Tension at break	3400 MPa	Tension at break	2150 MPa
Elongation at break	4.80%	Elongation at break	3.75%
EC 130 LV Epoxy resin + W340 hardener (weight ratio 100:37) produced by ALTANA VARNISH-COMPOUNDS		**EC 15 Epoxy resin + W152 MLR hardener (weight ratio 100:30) produced by ELANTAS**	
Density	1.14–1.16 g/mL	Density	1.08–1.12 g/mL
Young modulus	2900–3100 MPa	Young modulus	3100–3500 MPa
Tension at break	75–80 MPa	Tension at break	68–76 MPa
Elongation at break	8.5–9%	Elongation at break	3.0–8.0%

Notches of different geometries have been made on the specimens. In particular, the specimens of geometry I, II and III are shown in Figure 1 and were obtained from panel 1 (specimens AA01, AA02 and AA03) [19] while those of geometry IV and V (Figure 2) were obtained from panel 2 (specimens A4 and A11) [20]. Table 2 shows the dimensional characteristics and the theoretical notch coefficient k_t, which is a measure of the severity of the notch itself.

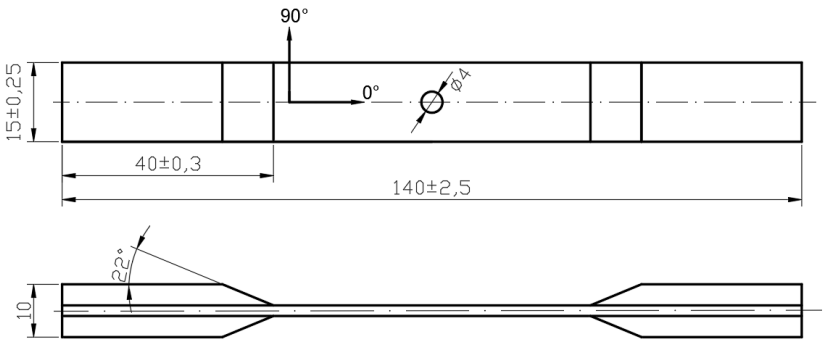

(**a**) Geometry I with a circular notch (named AA01)

Figure 1. *Cont.*

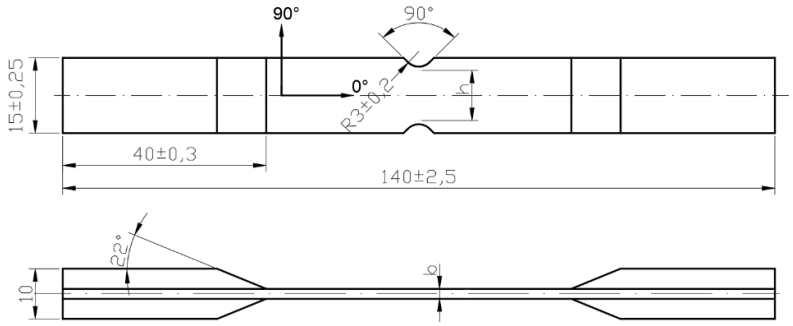

(**b**) Geometry II with V-notch (called AA02)

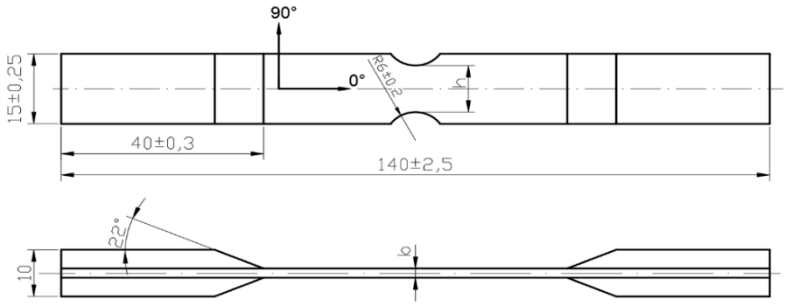

(**c**) Geometry III with soft U notch (called AA03)

Figure 1. Specimens obtained from panel 1.

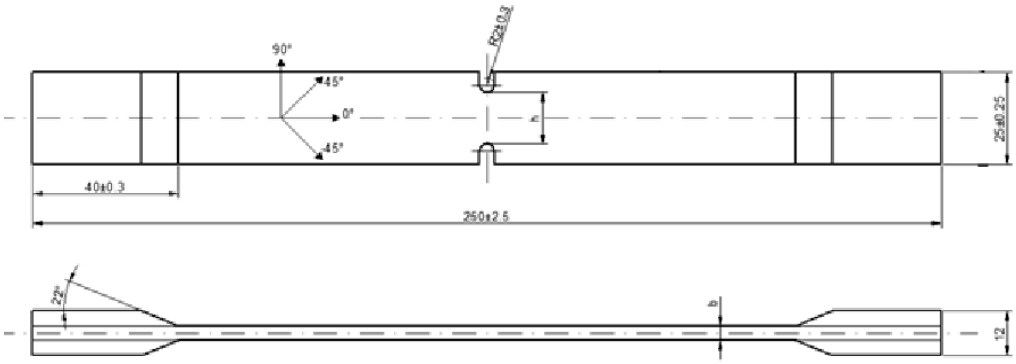

(**a**) Geometry IV with severe U notch (called A4).

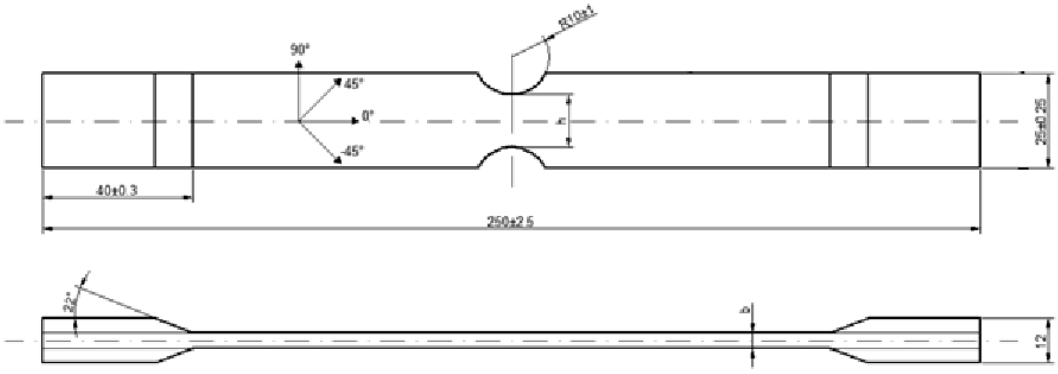

(**b**) Geometry V with soft U notch (called A11)

Figure 2. Specimens obtained from panel 2.

Table 2. Dimensional characteristics of the specimens.

Specimen	h [mm]	b [mm]	Net Section [mm^2]	k_t
AA01	*11.004*	*2.253*	*24.79*	*2.41*
AA02	*9.103*	*2.211*	*20.13*	*1.71*
AA03	*10.117*	*2.197*	*22.23*	*1.46*
A4	*14.271*	*4.025*	*57.44*	*2.35*
A11	*13.296*	*4.126*	*54.86*	*1.48*

Fatigue tests were performed applying several increasing load steps on the same specimen [21]. During each step, the temperature trend has been recorded to reveal both stationary temperature variation for each load block and to monitor the crack rise and evolution. The specimen areas with damage accumulation are always characterized by dissipative phenomena clearly evident in temperature maps.

To carry out the *stepped loading procedure*, the test characteristic parameters must be chosen to obtain a sufficient number of steps, which effectively describe the thermal response of the specimen, and single-step duration such as to avoid the accumulation of fatigue damage. In this procedure, there are basically two problems, namely choosing a value of the load increase between the steps, to obtain a sufficient number of steps that can appropriately describe the thermal response of the specimen and set an appropriate number of cycles for each step. The optimal duration of the test has two conflicting needs: on the one hand, it must be high enough to stabilize the thermal response and to obtain the limit temperature; on the other hand, it must be short enough to neglect the damage accumulation effect on the subsequent steps.

The choice of the initial load level depends on the mechanical properties of the material and must be lower than the fatigue limit to obtain a sufficient number of steps (about eight/nine steps). Obviously, this value is not known a priori. There are several experimental formulas designed to determine the initial load level according to the material; the simplest one consists of choosing a starting level equal to a fraction of the ultimate tensile strength with increments per step equal to $5 \div 10\%$ of the same.

A stress ratio equal to R = 0.1 was imposed. Then, an appropriate loading sequence was chosen, making sure that the increase in amplitude σ_a guaranteed an adequate number of steps. The load blocks sequence, whose choice was derived from the static tensile stress [20,22], is shown in Figure 3, for panel 1 and 2.

The duration of every single step has been set at 5000 cycles, based on previous experience. This compromise value avoids the accumulation of damage on the subsequent steps while still allowing the extrapolation of the stabilization temperature of the specimen. As regards the load frequency, the 10 Hz value was chosen to make heat exchange more evident. Fatigue tests were carried out using a universal servo-hydraulic testing machine (MTS 810) with a 100 kN load cell.

Monitoring the tests employing a thermal camera, it is possible to create a thermal map of the specimen throughout the test. An infrared thermal imaging FLIR camera, model SC 7500M, was used to acquire the thermal images. The thermal camera was equipped with a Focal Plane Array sensor, cooled using a Stirling cycle, having a NETD resolution of 25 mK; the detector acquires 320×256 pixels, being able to reach an image acquisition frequency (frame rate) of 383 Hz (see Figure A3 in Appendix A for set-up details).

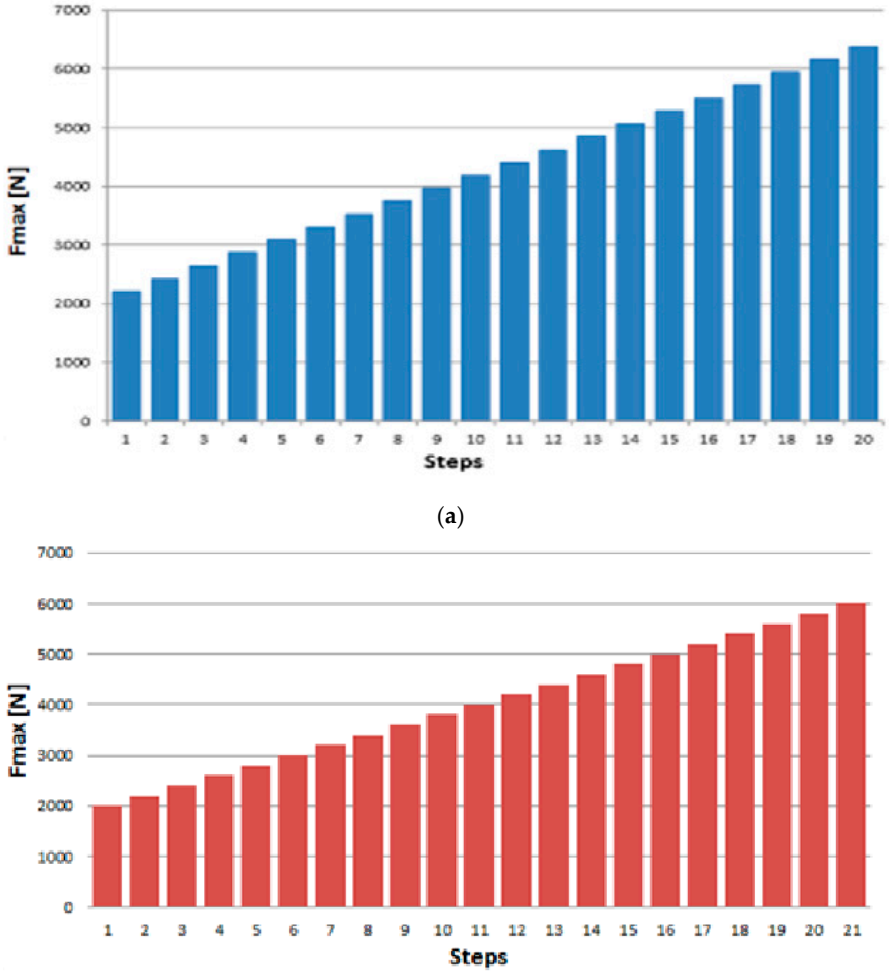

Figure 3. Step test: indication of the load for each step for Panel 1 (**a**) and Panel 2 (**b**).

During the test, there will be an area, called the hot zone, in which an increase in temperature will develop, easily identifiable in the case of a notched specimen and coincident with the root of the notch. The position and the size of a rectangular area is chosen to include the hottest area, that is, the area where peak temperature occurs. The rectangular area is the same for all steps and the temperature is averaged in this area. Strictly, one pixel should be selected, but this choice is not suitable for two reasons: firstly, it is difficult to individuate exactly the pixel with T_{max}, and secondly it is not assured that the pixel is the same for all steps. Therefore, a rectangular area has been chosen in order to catch the phenomenon minimizing the scatter. This area as evident from the first cycles, especially as the stress amplitude increases, hosts the first damage and, most likely, the break. The identification of the hot zone is made by examining the heat map in a generic instant of timeframe and determining two opposite vertices of a rectangle that contains it. Figure 4 shows as an example the thermal maps during the last test steps for specimen A4. The non-uniform heating in the net section is due to the non-perfectly symmetric geometry of the specimen (manufacturing tolerances) and to the unavoidable alignment error in the specimen gripping. In Figure 5, the coordinates of the hot zone for the specimen AA02 are shown. It is interesting to note in this case that the specific layup of the specimen $[0\ 90\ 90\ 0]_{x4}$ and the presence of the notch determines that the hot zone is not localized in the net section but in the zone where the 0° fibers are interrupted immediately before notch. This is a clear example of the complexity arising from the notch effect in composite, which is the result of not only the notch geometry but also and the local orientation of the

fibres in the high stress zone. The individuation of the stress state that causesthe dissipative phenomena, experimentally measured by IR camera, cannot avoid the physical presence of fibre and matrix adopting a mesoscale modelling [23]. In this particular case, stress acting on 0° layers must be transferred to 90° layers through interlaminar shear stress, thus determining a local increase of the stress state, which will constitute the nucleation zone of the fatigue failure. The prediction of the fatigue failure propagation in composite materials is more complex than homogeneous material, since the crack propagation path is governed not only by stress state but also by laminae orientation. Although dissipative phenomena are originated inside the material, the thermal energy is quickly diffused due to the limited thickness and a surface temperature variation is observed.

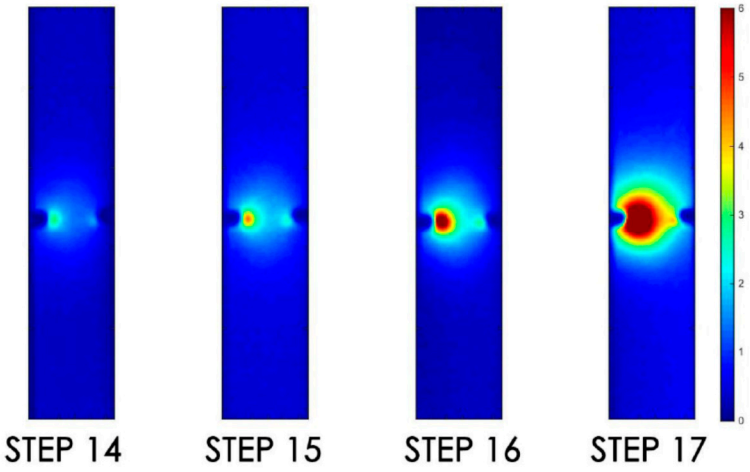

Figure 4. Thermal maps during the last steps of the test for specimen A4.

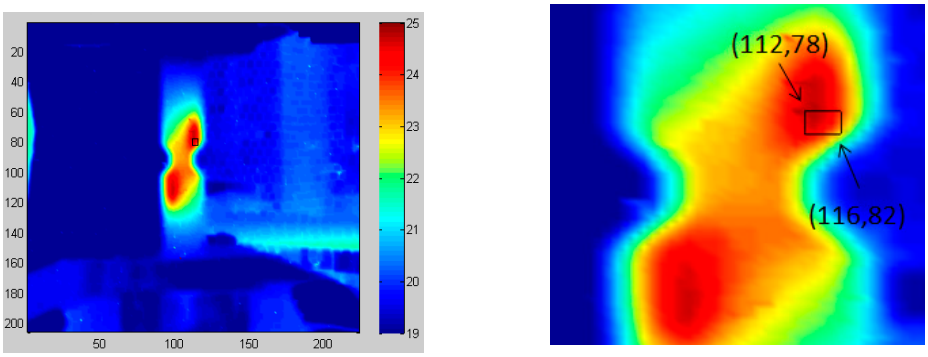

Figure 5. Identification of the hot zone (specimen AA02).

The correlation between the number of cycles and frames can be easily obtained from the acquisition frequency of the thermal camera, which was set at 1 Hz; therefore, 1 frame corresponds to 10 cycles.

Parallel to the hot zone, an area of the specimen sufficiently far from the notch is analysed, which is called the cold zone. It is a region that does not resent the notch effect. This area is of fundamental importance for the purposes of the analysis, as it has been shown that the temperature trend of this area perfectly coincides with that of the analogue specimen without a notch [21]. This suggests a way to determine the fatigue notch coefficient. In fact, by examining the hot zone and the cold zone of the same notched specimen, it is possible to obtain the fatigue limit, as well as the fatigue limit of the corresponding smooth specimen, with evident savings in time and costs, having to analyse only one sample. The fatigue notch coefficient can be obtained very simply as the ratio of these two fatigue limits.

The identification of the cold zone occurs in the same way as the hot zone (see Figure A4 in Appendix A for coordinate details).

3. Results and Discussion

This section shows the steps performed during the processing, through software, of the thermal data on the specimen surface, to obtain the stabilization temperature and the fatigue limit.

A Matlab script was implemented to open and process the .asc files, exported from the Altair thermal camera acquisition software. This file has a data structure similar to a three-dimensional matrix, in which the third dimension is represented by the acquired frames, or in other words by time. Each plane of the matrix represents, however, the thermal image where the rows and columns identify the coordinates of each point of the specimen in a specific frame, to which the corresponding temperature value is associated.

The frames acquired for each step are 500 (i.e., 5000 load cycles) while the thermal image returned by the thermal imaging camera has a resolution of 360 × 256. This implies that the 3D matrix is of the type [360 × 256 × 500]. Therefore, the script allows determining the average temperature increase (i.e., averaged over the pixels) of an area of interest, normalized concerning the value of the initial instant, as the frames vary. The trend is reported in a ΔT-N graph, where N is the number of cycles, obtained by multiplying the number of frames by a factor of 10 (being 10 Hz the load frequency), as a result of the previous settings on the thermal camera.

At this point, the script proceeds with the calculation of the limit temperature, always as ΔT, through a non-linear least-squares fitting. At the same time, the data are exported to the Mathematica environment, to perform a more specific analysis where necessary. In this case, the optimization allows normalizing the residues in order not to incur in estimation errors due to the shift or drift of the trend. This processing is repeated for all specimen geometries, both taking into consideration the hot and cold areas. Figures 6 and 7 show an example of what has been achieved for AA03 specimen for hot and cold zones considering only the higher load steps. A brief discussion is required to justify the statistical treatment carried out by data processing. At lower loads, in fact, thermal data are characterized by a higher scatter, especially in the cold zone (Figure 7). The problem is represented by the fact that at lower loads ΔT falls in the thermocamera resolution range. At higher loads, that are the most significant, the scatter vanishes. Since the physical phenomenon that originated the temperature change is the same, the exponential law, which is typical of the thermal phenomena, is correctly assumed for the thermal behaviour at higher loads. In these cases, experimental data justifies this assumption. For lower loads, where experimental data would not allow assuming an exponential law effectively, it is reasonable to infer that the same law governs the physical phenomenon, justifying the adopted procedure.

Once the limit temperature values have been obtained, a further script is used, which allows diagramming these values with the corresponding stress levels. Subsequently, the asymptotes are traced, as described in the procedure [1], and the fatigue limits are identified. In Figure 8, the result of this operation is shown for specimens AA03 as an example. The stress values have been obtained considering the net section in the hot area and the gross section in the cold area. Moreover, the steps considered for the hot and cold zones are not the same since in the gross section, the damage occurs at higher loads.

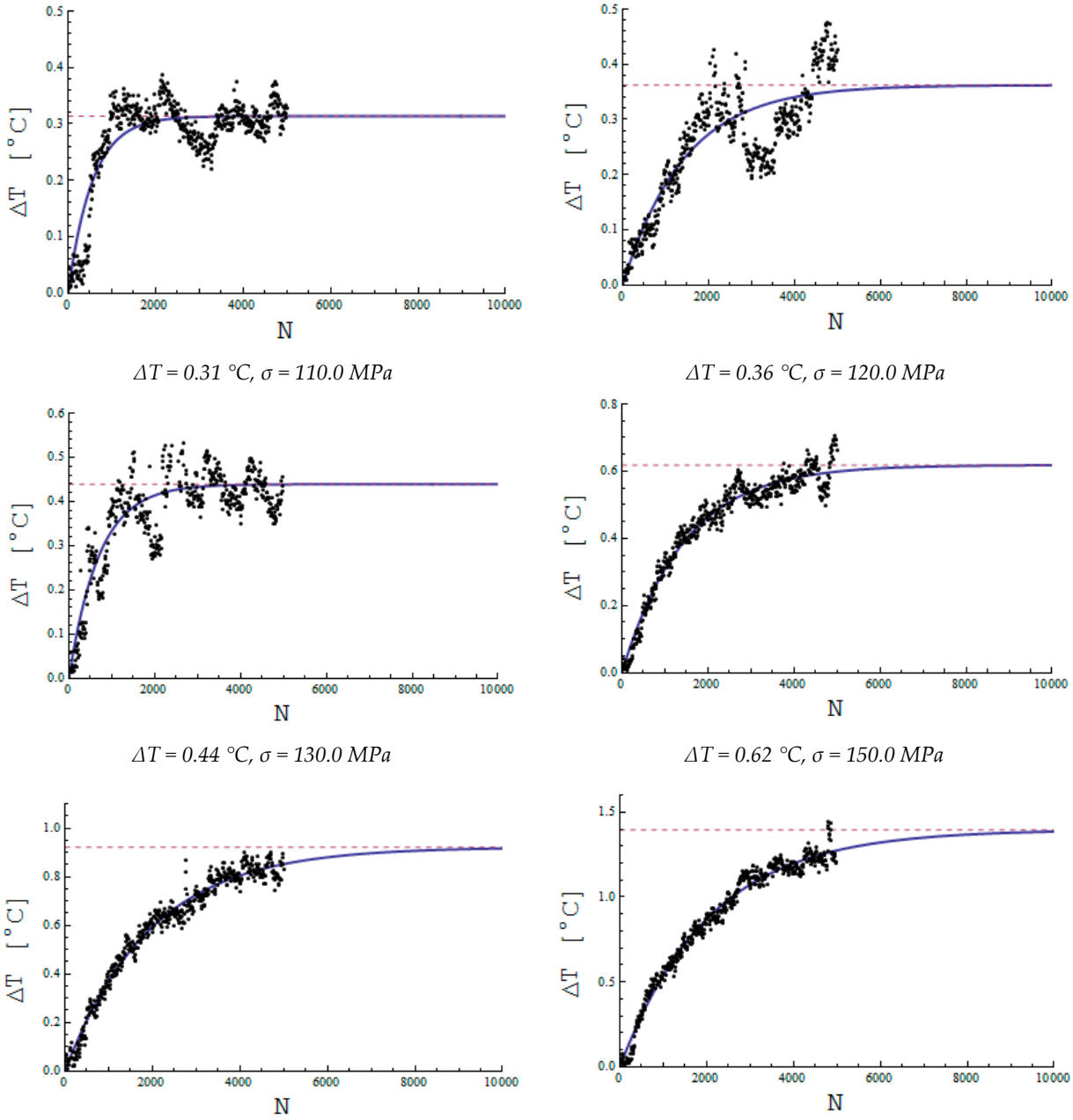

Figure 6. Identification of the limit temperature by least-squares interpolation at different load steps (specimen AA03 hot zone).

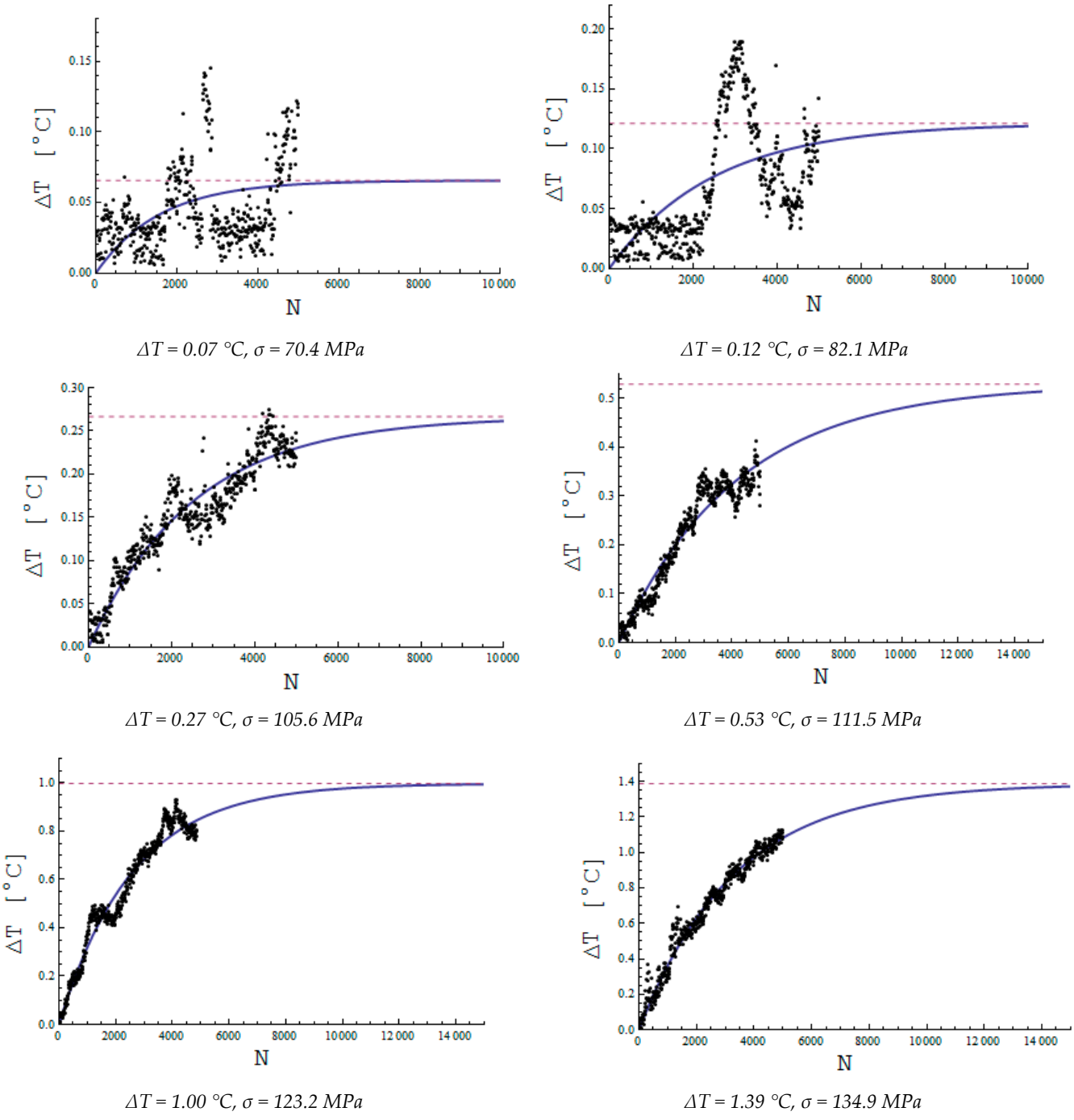

Figure 7. Identification of the limit temperature by least-squares interpolation at different load steps (specimen AA03 cold zone).

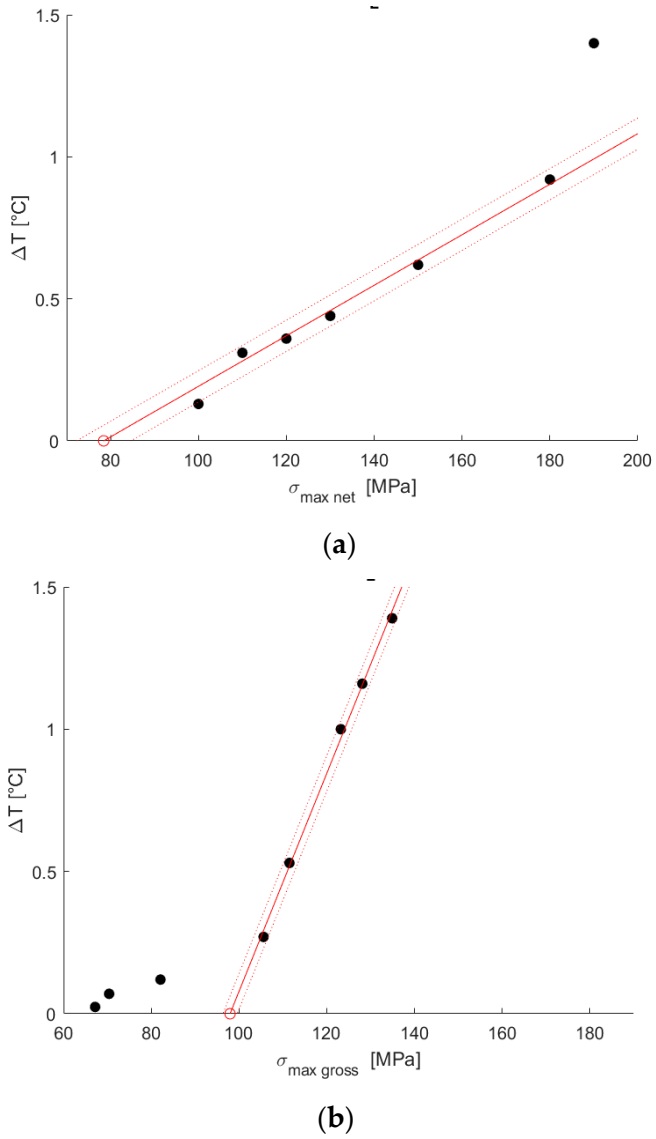

Figure 8. Identification of the fatigue limit for specimen AA03 for (**a**) hot zone, (**b**) cold zone.

Table 3 reports the resulting fatigue limits for notched and smooth specimens, i.e., for hot and cold areas, respectively. The fatigue limit, as known, is influenced by the notch geometry, as well as being specific to the material analysed. Therefore, in the case of a smooth specimen, it is correct that the fatigue limit remains unchanged for specimens obtained from the same laminate. This result confirms the reliability of the technique.

Table 3. Fatigue limits and k_f coefficient for different notch geometries.

	Fatigue Limit [N/mm^2]		
Specimen	**Hot Area (Notched)**	**Cold Area (Smooth)**	**k_f**
AA01	119.2	98.1	0.823
AA02	75.8	97.7	1.289
AA03	78.4	97.9	1.249
A4	46.0	51.9	1.127
A11	43.3	50.4	1.165

Once the values of the fatigue limit for smooth and notched specimens have been obtained, it is possible to estimate the fatigue notch coefficient for each type of notch by simply carrying out the ratio between the fatigue limits obtained with the thermographic technique. Table 3 shows the k_f values for each type of material and notch geometry.

These results are comparable with the values obtained in [23] by Quaresimin, who studied the fatigue behaviour of composite materials in the presence of a notch for different lay-ups and types of stress, using the traditional Wöhler curve technique. It can be noted that in the case of a specimen with a hole, the fatigue behaviour is even improved by the presence of the notch.

First of all, it can be observed that the values of the coefficients for the five types of geometry examined are relatively small, despite a non-negligible theoretical notch coefficient in some cases. This indicates low notch sensitivity in the case of a composite subject to fatigue load even in the presence of severe geometries, or in other words, the presence of the notch weakly influences the fatigue behaviour of the composite material. This was also found in [24] in the case of R = 0.05, a value very close to the case examined in the present work. In the case of traction-compression stress (R = −1), on the other hand, the sensitivity is increased, due to the local microbucklings that feed the damage phenomenon. In the case of the hole specimen, the k_f is lower than 1, a result that at first glance could be anomalous but which has a justification in the fact that the evolution of damage at the edge of the hole produces a considerable reduction in the concentration of tension. This is related to the fact that the laminates analysed have a fibre-dominated behaviour [24]. This type of materials, in the case of tensile-tensile loading, have a low sensitivity to the fatigue and present very flat fatigue curves; this is due to the random failure of the fibres, which is similar to that happening in unidirectional composites.

However, as affirmed in [25,26], the notched fatigue strength of the laminates in short-life range is lower than the unnotched fatigue strengths towing to a notch-based reduction in static strength. In the long-life range, the notch effect vanishes since its sensitivity in a composite material is reduced by material degradation and plastic deformation in its proximity with consequent stress redistribution at its tips [27]. This behaviour is confirmed in [28,29] where the authors confirm that the fatigue behaviour of composite material is less affected by the notch effect over 10^6 cycles, and the stress concentration effect is noted only for lower fatigue lives. Although, in theory, the notch affects the fatigue resistance of a composite material less significantly than traditional material, the value of the fatigue notch coefficient is still different from the unit (Table 3); in particular, they are higher than 1 except in one case: this means that the presence of a notch is not negligible in the short-life range i.e., at higher fatigue loads.

Regarding the evaluation of the fatigue limit, it is observed that the specimens obtained from the first panel have greater resistance than those obtained from the second panel. This is due to the stacking sequence of the composite, which in the first laminate has two layers in the 0° direction, which is the main stress direction in the case of a tensile test. Given the absence of data on the fatigue limit in the literature, a traditional test was carried out to check on the results obtained and validate the used technique. In particular, the specimens of geometry V were tested, given the higher number of samples available. The Wöhler curve is shown in Figure 9, obtaining a fatigue limit for $N = 10^7$ cycles equal to 60 MPa.

It can be seen that the value differs from that obtained with the Risitano technique which provides the fatigue limit for *infinite* life. In particular, the fatigue limit obtained with thermographic methods is 30% lower than that traditionally obtained. The fixed number of cycles is arbitrary since it depends on numerous factors, primarily based on the material. Obviously, the estimation improves by increasing this value.

Finally, it is possible to demonstrate that what has been done through the limit temperature can also be obtained considering the temperature rise v_T, which is the slope of the initial trait of the temperature trend. Figure 10 shows the fatigue limit calculation based on temperature rate for notched specimens AA03 and A4, obtaining a fatigue limit equal to 79.1 MPa for AA03 and 45.8 MPa for A4. The last points are neglected since they

deviate significantly from the previous ones; this indicates that the specimen is close to rupture. By comparing these values of the fatigue limits with values in Table 3, a negligible percentage difference, lower than 1%, was found.

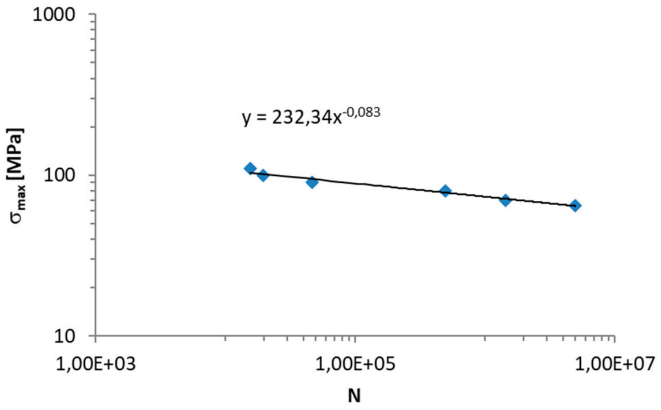

Figure 9. Wöhler curve obtained according to the traditional method.

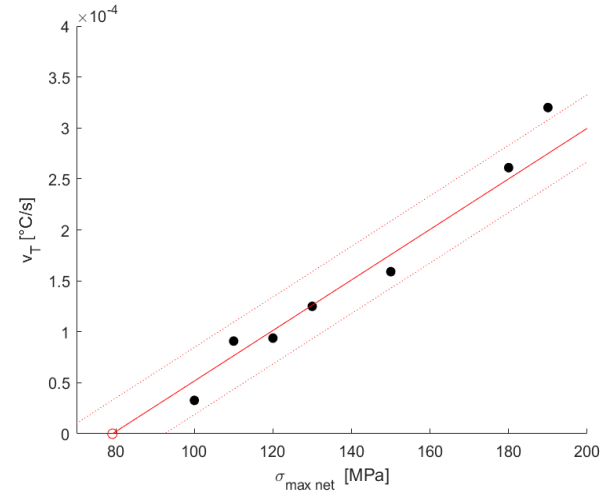

(**a**)

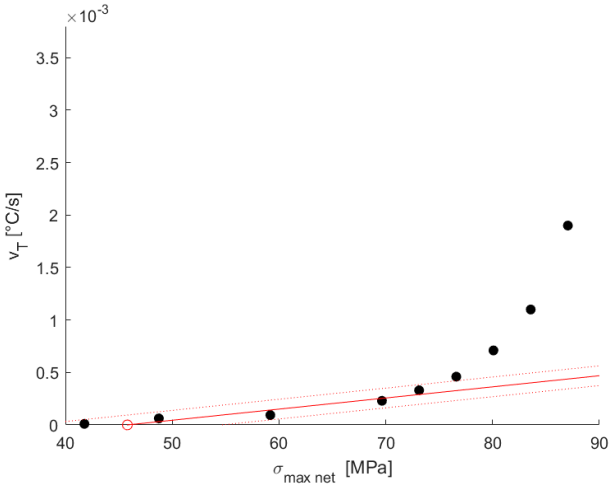

(**b**)

Figure 10. Fatigue limit identification for specimens AA03 (**a**) and A4 (**b**) based on temperature rise v_T.

4. Conclusions

In this work, the fatigue notch coefficient was evaluated on composite materials, using a technique based on thermographic measurements. The adopted method allows quickly determining the fatigue limit of a material, without the need to carry out destructive fatigue tests. The technique, widely verified in the case of traditional materials, has been tested here on composite material configured in two different lay-ups. Notched specimens have been fatigue tested according to the load steps procedure under alternate tension–tension loads.

The originality of this work includes, first, the development of a procedure for rapid determination of the fatigue notch coefficient that can be applied to various types of materials. Moreover, the value of this coefficient has been numerically determined for different notch geometries and different types of composite laminates representing an example of how this technique could rapidly lead to an evaluation of k_f. Finally, it has been demonstrated that the used technique can be improved considering the temperature rise rather than the limit temperature as a reference parameter allowing to further reducing the time of the test. The future outlook of the study is to collect in a fast way additional k_f values for different laminates and notch geometries.

Author Contributions: Conceptualization, M.D.G.; methodology, M.D.G.; formal analysis and investigation, M.D.G., F.P. and R.N.; writing—original draft preparation, M.D.G. and F.P.; writing—review and editing, M.D.G., F.P. and R.N.; supervision, M.D.G. All authors have read and agreed to the published version of the manuscript.

Funding: This research received no external funding.

Institutional Review Board Statement: Not applicable.

Informed Consent Statement: Not applicable.

Data Availability Statement: Not applicable.

Conflicts of Interest: The authors declare no conflict of interest.

Appendix A

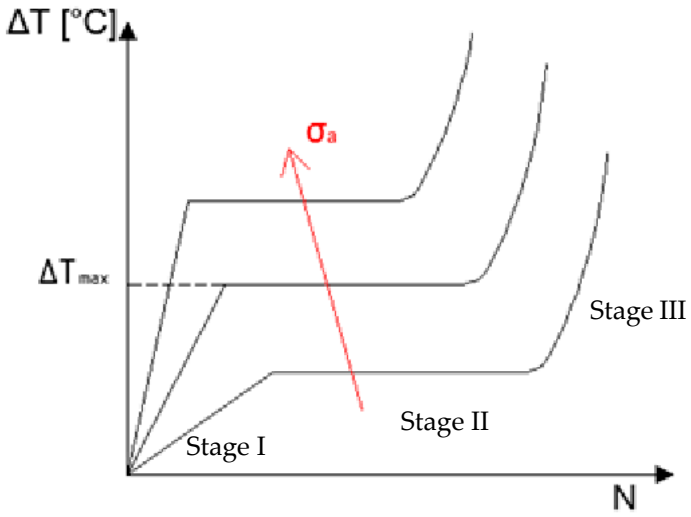

Figure A1. Temperature qualitative trend of a specimen point for a step test.

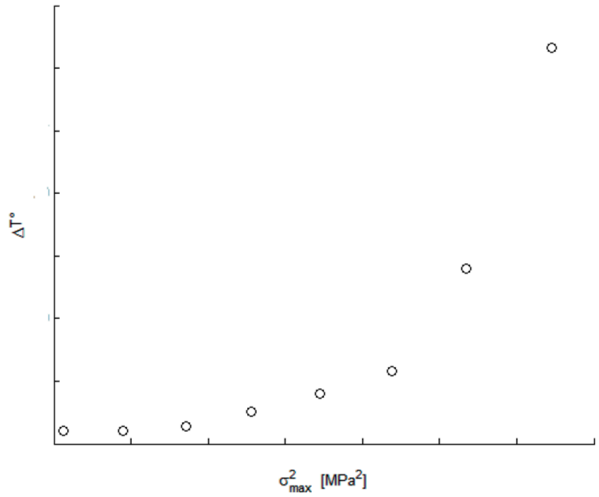

Figure A2. Diagram resulting from a step test with the maximum load applied on the abscissa axis, or its square, and the temperature increases on the ordinates.

Figure A3. Fatigue test set-up.

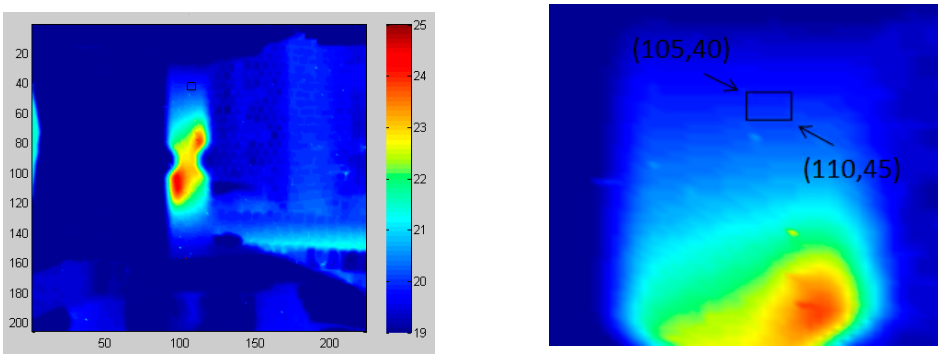

Figure A4. Identification of the cold zone (specimens AA01-AA02-AA03).

References

1. La Rosa, G.; Risitano, A. Thermographic methodology for rapid determination of the fatigue limit of materials and mechanical components. *Int. J. Fat.* **2000**, *22*, 65–73. [CrossRef]
2. Meneghetti, G.; Ricotta, M.; Risitano, G.; Risitano, A.; Atzori, B.; Guglielmino, E. Fatigue limit evaluation of a stainless steel using thermal data analysis. In Proceedings of the ICF 2017—14th International Conference on Fracture, Rhodes, Greece, 18–23 June 2017; pp. 636–637.

3. Fargione, G.; Geraci, A.; La Rosa, G.; Risitano, A. Rapid determination of the fatigue curve by the thermographic method. *Int. J. Fat.* **2002**, *24*, 11–19. [CrossRef]
4. Ancona, F.; De Finis, R.; Galietti, U.; Palumbo, D. Caratterizzazione a fatica mediante tecnica termografica: Una nuova robusta procedura di analisi dei dati. In Proceedings of the 44° Convegno Nazionale AIAS (Associazione Italiana Per L'analisi Delle Sollecitazioni), Università di Messina, Messina, Italy, 2–5 September 2015.
5. De Finis, R.; Palumbo, D.; Ancona, F.; Galietti, U. Fatigue limit evaluation of various martensitic stainless steels with new robust thermographic data analysis. *Int. J. Fat.* **2015**, *96*, 74–88.
6. Rigon, D.; Ricotta, M.; Meneghetti, G. Analysis of dissipated energy and temperature fields at severe notches of AISI 304L stainless steel specimens. *Frat. Integrità Strutt.* **2019**, *47*, 334–347. [CrossRef]
7. Wang, X.G.; Crupi, V.; Guo, X.L.; Zhao, Y.G. Quantitative Thermographic Methodology for fatigue assessment and stress measurement. *Int. J. Fat.* **2010**, *32*, 1970–1976. [CrossRef]
8. Curà, F.; Curti, G.; Sesana, R. A New Iteration Method for the Thermographic Determination of Fatigue Limit In Steels. *Int. J. Fat.* **2005**, *27*, 453–459. [CrossRef]
9. Ricotta, M.; Meneghetti, G.; Atzori, B.; Risitano, G.; Risitano, A. Comparison of Experimental Thermal Methods for the Fatigue Limit Evaluation of a Stainless Steel. *Metals* **2019**, *9*, 677. [CrossRef]
10. De Finis, R.; Palumbo, D.; da Silva, M.M.; Galietti, U. Is the temperature plateau of a self-heating test a robust parameter to investigate the fatigue limit of steels with thermography? *Fatigue Fract. Eng. Mater. Struct.* **2018**, *41*, 917–934. [CrossRef]
11. Vergani, L.; Colombo, C.; Libonati, F. A review of thermographic techniques for damage investigation in composites. *Frat. Integrità Strutt.* **2014**, *27*, 1–12. [CrossRef]
12. Toubal, L.; Karama, M.; Lorrain, B. Damage evolution and infrared thermography in woven composite laminates under fatigue loading. *Int. J. Fat.* **2006**, *28*, 1867–1872. [CrossRef]
13. Meneghetti, G.; Quaresimin, M. Fatigue strength assessment of a short fiber composites based on the specific heat dissipation. *Compos. Part. B* **2011**, *42*, 217–225. [CrossRef]
14. Colombo, C.; Libonati, F.; Pezzani, F.; Salerno, A.; Vergani, L. Fatigue behaviour of a GFRP laminate by thermographic measurements. *Procedia Eng.* **2011**, *10*, 3518–3527. [CrossRef]
15. Demelio, P.G.; De Finis, R.; Galietti, U.; Palumbo, D. Fatigue Limit Evaluation of Composite Materials by Means of TSA. In Proceedings of the QIRT Conference, Gdansk, Poland, 4–8 July 2016.
16. Karama, M. Determination of the fatigue limit of a carbon/epoxy composite using thermographic analysis. *Struct. Control. Health Monit.* **2011**, *18*, 781–789. [CrossRef]
17. Bale, J.; Valot, E.; Polit, O.; Bathia, C.; Monin, M.; Soemardi, T. Thermal phenomenon of glass fibre composite under tensile static and fatigue loading. *J. Mech. Eng. Sci.* **2017**, *11*, 2755–2769. [CrossRef]
18. ASTM. *Standard Test Method for Tensile Properties of Polymer Matrix Composite Materials*; D 3039/D 3039M-00; ASTM: West Conshohocken, PA, USA, 2000; (Reapproved 2006).
19. Giancane, S.; Nobile, R.; Panella, F.W.; Dattoma, V. Damage evolution of composite laminates with Digital Image Correlation. *Key Eng. Mater.* **2011**, *452–453*, 377–380. [CrossRef]
20. Dattoma, V.; Giancane, S. Evaluation of energy of fatigue damage into GFRC through digital image correlation and thermography. *Compos. Part. B* **2013**, *47*, 283–289. [CrossRef]
21. Risitano, A.; Fargione, G. Experimental method for the determination of the under-stress first-plasticization process parameters. In Proceedings of the Convegno Nazionale IGF XXII, Roma, Italy, 1–3 July 2013; pp. 370–372.
22. Giancane, S.; Panella, F.W.; Nobile, R.; Dattoma, V. Fatigue damage evolution of fiber reinforced composites with digital image correlation analysis. *Procedia Eng.* **2010**, *2*, 1307–1315. [CrossRef]
23. Ghazimoradi, M.; Naouar, N.; Carvelli, V.; Boisse, P.; Frassine, R. Tetraxial textiles: Assessment of mesoscale mechanical modelling by experimental measurements. *IOP Conf. Ser. Mater. Sci. Eng.* **2018**, *406*, 12048. [CrossRef]
24. Quaresimin, M. Comportamento statico e a fatica di compositi tessuti. In Proceedings of the XXX Convegno Nazionale AIAS, Alghero, Italy, 12–15 September 2001.
25. Yi, X.; Du, S.; Zhang, L. Composite Materials Engineering, Volume 1. In *Fundamentals of Composite Materials*; Springer: Berlin/Heidelberg, Germany, 2018.
26. Hull, D. *Introduction to Composite Materials*; Cambridge University Press: Cambridge, UK, 1982.
27. Kawai, M.; Shiratsuchi, T. Vanishing notch sensitivity approach to fatigue life prediction of notched cross-ply CFRP laminates at room temperature. *J. Compos. Mater.* **2012**, *46*, 2935–2950. [CrossRef]
28. Jollivet, T.; Peyrac, C.; Lefebvre, F. Damage of composite materials. *Procedia Eng.* **2013**, *66*, 746–758. [CrossRef]
29. Reis, P.N.B.; Ferreira, J.A.M.; Antunes, F.; Costa, J.D.M. Fatigue Notch Sensibility of Thermoplastic Glass Fibre Composites. *Mater. Sci. Forum* **2006**, *514–516*, 653–656. [CrossRef]